Variational multiscale SGS modeling for LES using a high-order discontinuous Galerkin method

By K. Bando, F. Naddei†, M. de la Llave Plata† AND M. Ihme

1. Motivation and objectives

The use of high-order methods, in particular the discontinuous Galerkin (DG) method, has become increasingly popular for the simulations of turbulent flows. The low dissipation and dispersion errors associated with these high-order schemes make them attractive for scale-resolving computations, for which fine turbulent scales must be resolved for long periods of time integration. In addition, the compactness of the DG discretization is very well suited for modern high-performance computing architectures.

The accuracy of DG methods and the improvement of the simulation quality with increasing order of accuracy have been demonstrated for canonical test cases (Gassner & Beck 2013; Carton de Wiart *et al.* 2015) as well as more realistic configurations, such as the simulation of transitional flows (Bassi *et al.* (2016); Fernandez *et al.* (2017)). Most of these studies used the so-called implicit large-eddy simulation (LES) approach, for which no subgrid-scale (SGS) model term is formulated in the governing equations. The stability and accuracy of simulations rely solely on the inherent numerical dissipation associated with the employed stabilization method. In order to improve the robustness of DG methods, physics-based provably stable schemes have been a focus of research in the high-order community. Recent developments include provably entropy stable schemes at the discrete (e.g. Chen & Shu (2017)) or continuous (e.g. Hiltebrand & Mishra (2014)) levels. An entropy-bounded DG scheme (Lv & Ihme 2015) has been developed and successfully employed for the simulation of under-resolved compressible turbulence (Lv *et al.* 2018). The advantage of high-order accuracy was demonstrated in cases with low to moderate turbulent Mach numbers.

Even though the implicit LES (ILES) has shown promising results, the ability of the scheme to provide the correct level of SGS dissipation for arbitrary settings remains an open question. Moreover, it is expected that for highly turbulent flows, an SGS model will be required. The variational formulation of the DG discretization is well suited for a variational multiscale (VMS) SGS model that has been pioneered by Hughes *et al.* (2000). It has been successfully used in the context of spectral methods and mixed finite volume/finite element methods for incompressible and compressible flow simulations. Recently, a VMS-LES approach combined with a modal DG framework was proposed by Chapelier *et al.* (2016). In this study, a VMS SGS model was successfully used to simulate the Taylor-Green vortex problem, showing improved results over the Smagorinsky or no-model approach, when compared to filtered reference DNS data.

The objective of the present study is to investigate this VMS SGS model for the simulations of compressible turbulence at moderate turbulent Mach number conditions. In particular, the ability of the model to stabilize solutions and the effect of the *a-priori*

† Department of Aerodynamics, Aeroelasticity and Acoustics, ONERA, France

scale separation on the SGS energy transfer are investigated. Results are compared with an ILES approach using the entropy-bounded DG scheme (Lv & Ihme 2015).

2. Mathematical formulation

2.1. *Governing equations*

In the context of VMS-LES, several approaches exist for deriving the governing equations. In the foundational work of Hughes *et al.* (2000) and subsequent papers, this formulation was derived through a variational projection of the Navier-Stokes equations, which requires the selection of a scale separation framework (large-small or large-small-unresolved). For the compressible case, this approach leads to a large number of terms (Farhat *et al.* 2006) that are eventually neglected using a scale separation argument or modeled. In the present work, we follow the approach adopted in Chapelier *et al.* (2016) that uses the filtered LES equations based on the LES formalism of Lesieur & Compte (2001). Both approaches lead to the same final set of equations when projected to the test function space with the addition of an unclosed term that is modeled in the same fashion.

Filtered conservation equations for mass, momentum, and energy are written in a compact form as

$$\partial_t \mathbf{U} + \nabla \cdot \mathbf{F} = \nabla \cdot \mathbf{Q} + \nabla \cdot \mathbf{Q}_{\text{SGS}}, \tag{2.1}$$

where

$$\begin{gathered} \mathbf{U} = \begin{pmatrix} \overline{\rho} \\ \overline{\rho}\widetilde{\boldsymbol{u}} \\ \overline{\rho}\widetilde{E} \end{pmatrix}, \ \mathbf{F} = \begin{pmatrix} \overline{\rho}\widetilde{\boldsymbol{u}}^T \\ \overline{\rho}\widetilde{\boldsymbol{u}} \otimes \widetilde{\boldsymbol{u}} + \overline{P}\mathbf{I} \\ \left(\overline{\rho}\widetilde{E} + \overline{P}\right)\widetilde{\boldsymbol{u}}^T \end{pmatrix}, \\ \mathbf{Q} = \begin{pmatrix} 0 \\ \boldsymbol{\tau} \\ -\boldsymbol{q}^T + (\boldsymbol{\tau} \cdot \widetilde{\boldsymbol{u}})^T \end{pmatrix}, \ \mathbf{Q}_{\text{SGS}} = \begin{pmatrix} 0 \\ \boldsymbol{\mathcal{T}}^D \\ -\boldsymbol{q}_{\text{SGS}}^T \end{pmatrix}. \end{gathered} \tag{2.2}$$

In the above equations, $\mathbf{U}$, $\mathbf{F}$, $\mathbf{Q}$, and $\mathbf{Q}_{\text{SGS}}$ denote, respectively, the conservative variables solution vector, the inviscid flux, the viscous flux, and the SGS flux. $\boldsymbol{\mathcal{T}} = -\overline{\rho\boldsymbol{u} \otimes \boldsymbol{u}} + \overline{\rho}\widetilde{\boldsymbol{u}} \otimes \widetilde{\boldsymbol{u}}$ is the subgrid stress tensor and $\boldsymbol{\mathcal{T}}^D$ its deviatoric part. The spherical part $\text{tr}(\boldsymbol{\mathcal{T}})\mathbf{I}$ is absorbed into the pressure to form the macropressure $\overline{P} = \overline{p} - \text{tr}(\boldsymbol{\mathcal{T}})/3$. The SGS heat flux becomes

$$\boldsymbol{q}_{\text{SGS}} = \overline{(\rho E + p)\boldsymbol{u}} - (\overline{\rho}\widetilde{E} + \overline{P})\widetilde{\boldsymbol{u}}. \tag{2.3}$$

The viscous stress tensor and the conductive heat flux are written as

$$\boldsymbol{\tau} = \mu(\widetilde{\theta}) \left[\nabla\widetilde{\boldsymbol{u}} + (\nabla\widetilde{\boldsymbol{u}})^T - \frac{2}{3}(\nabla \cdot \widetilde{\boldsymbol{u}})\mathbf{I} \right], \tag{2.4}$$

$$\boldsymbol{q} = -\lambda \nabla\widetilde{\theta}, \tag{2.5}$$

with $\widetilde{\theta} = \widetilde{T} - \text{tr}(\boldsymbol{\mathcal{T}})/(2\overline{\rho}C_v)$ being the macrotemperature (the dependence with respect to the macrotemperature is an ad-hoc assumption). The thermal conductivity λ is computed using the molecular Prandtl number. The system is closed with the ideal gas relation

$$\overline{P} = \overline{\rho}R_g\widetilde{\theta} + \frac{3\gamma - 5}{6}\text{tr}(\boldsymbol{\mathcal{T}}), \tag{2.6}$$

where γ is the ratio of specific heat coefficients, R_g is the specific gas constant, and

the last term on the right-hand side, which is neglected, arises from the fact that the macrotemperature has been defined such that $\overline{\rho}\widetilde{E} = \overline{\rho}C_v\widetilde{\theta} + \overline{\rho}||\widetilde{\boldsymbol{u}}||^2/2$.

The main advantage of this LES formulation is that it only requires the addition of an SGS term when a compressible Navier-Stokes solver is available. The terms modeling the effect of the unresolved scales on the resolved scales are introduced at the same time as the VMS formulation.

2.2. *DG discretization*

The spatial domain Ω is first partitioned into N_e elements $\{\Omega_e\}$, and the following broken space is introduced as the approximation functional space

$$\mathcal{V}_h^p = \{\phi \in L^2(\Omega) \mid \phi|_{\Omega_e} \in \mathcal{P}_p(\Omega_e),\ \forall \Omega_e\}. \tag{2.7}$$

Let $\{\phi_i\}_{i=1\ldots N_p}$ denote a basis of $\mathcal{V}_h^p$. The discrete solution vector is sought in the form

$$\mathbf{U} \simeq \mathbf{U}_h = \sum_{i=1}^{N_p} \mathbf{U}_{h,i}(t)\phi_i(x). \tag{2.8}$$

Since in this study only hexahedral meshes are considered, the most natural basis functions suited for a VMS SGS model in a DG framework are the Legendre polynomials (orthonormal hierarchical basis). Therefore, the tensor product of 1D Legendre polynomials is considered. Equation (2.1) is then multiplied by a test function $\phi \in \mathcal{V}_h^p$ and integrated over the domain Ω to obtain the discretized variational form. For clarity, the inviscid and viscous parts are introduced separately, and the SGS term is introduced when considering the VMS formulation.

The inviscid part reads

$$\begin{gathered}\int_\Omega \phi(\partial_t \mathbf{U} + \nabla\cdot\mathbf{F}(\mathbf{U}))\ d\Omega = \\ \sum_e \left[\int_{\Omega_e} \phi\partial_t\mathbf{U}\ d\Omega - \int_{\Omega_e} \mathbf{F}(\mathbf{U})\cdot\nabla\phi\ d\Omega + \oint_{\partial\Omega_e} \phi^+\mathbf{F}(\mathbf{U})\cdot\widehat{\boldsymbol{n}}\ d\Gamma\right] \simeq \\ \sum_e \left[\int_{\Omega_e} \phi\partial_t\mathbf{U}_h\ d\Omega - \int_{\Omega_e} \mathbf{F}(\mathbf{U}_h)\cdot\nabla\phi\ d\Omega + \oint_{\partial\Omega_e} \phi^+\widehat{\mathbf{F}}(\mathbf{U}_h^+, \mathbf{U}_h^-, \widehat{n})\ d\Gamma\right],\end{gathered} \tag{2.9}$$

where $\widehat{\boldsymbol{n}}$ denotes the outward unit normal vector; $+$ and $-$ superscripts denote an interior and exterior quantity, respectively; and $\widehat{\mathbf{F}}$ is the inviscid numerical flux. In this study, a local Lax-Friedrichs flux is used.

The viscous part is discretized using the BR2 formulation (Bassi & Rebay 2000). A slightly different but equivalent approach is introduced here in order to stress the role of the lifting operator, which is important for post-processing. First, an auxiliary variable $\boldsymbol{\vartheta}$ is introduced, and the original (second-order) Eq. (2.1) is recast into two first-order equations (the SGS term that takes a form similar to the viscous flux is omitted for clarity)

$$\begin{cases} \boldsymbol{\vartheta} = \mathbf{Q}, \\ \partial_t\mathbf{U} + \nabla\cdot\mathbf{F} = \nabla\cdot\boldsymbol{\vartheta}, \end{cases} \tag{2.10}$$

and the viscous flux is linearized with respect to the state gradient

$$\boldsymbol{\vartheta} = \boldsymbol{\mathcal{A}} : \nabla\mathbf{U}. \tag{2.11}$$

The first line of Eq. (2.10) is multiplied by $\phi \in \mathcal{V}_h^p$ and integrated by parts

$$\begin{aligned}\int_\Omega \boldsymbol{\vartheta}\phi \; d\Omega &= \sum_e \int_{\Omega_e} \boldsymbol{\vartheta}\phi \; d\Omega \\ &= \sum_e \left[- \int_{\Omega_e} [\nabla \cdot (\boldsymbol{\mathcal{A}}\phi)] \cdot \mathbf{U} \; d\Omega + \oint_{\partial\Omega_e} \phi^+ \boldsymbol{\mathcal{A}} : (\mathbf{U} \otimes \widehat{\boldsymbol{n}}) \; d\Gamma \right].\end{aligned} \tag{2.12}$$

Introducing the discretization and integrating by parts one more time leads to

$$\begin{aligned}\int_\Omega \boldsymbol{\vartheta}\phi \; d\Omega &\simeq \int_\Omega \boldsymbol{\vartheta}_h\phi \; d\Omega \\ &= \sum_e \left[\int_{\Omega_e} (\boldsymbol{\mathcal{A}} : \nabla_h \mathbf{U}_h)\phi \; d\Omega + \oint_{\partial\Omega_e} \phi^+ \boldsymbol{\mathcal{A}}^+ : ((\widehat{\mathbf{U}} - \mathbf{U}_h^+) \otimes \widehat{\boldsymbol{n}}) \; d\Gamma \right].\end{aligned} \tag{2.13}$$

Therefore,

$$\boldsymbol{\vartheta}_h|_{\Omega_e} = \mathscr{P}(\boldsymbol{\mathcal{A}} : \nabla_h \mathbf{U}_h) + r_e(\boldsymbol{\mathcal{A}} : ((\widehat{\mathbf{U}} - \mathbf{U}_h^+) \otimes \widehat{\boldsymbol{n}})), \tag{2.14}$$

where $\mathscr{P}$ is the projection onto the discrete space and r_e is the lifting operator, which operates from the space of functions defined on the faces to the test function space and can be computed in element Ω_e as

$$\int_{\Omega_e} \phi r_e(\varphi) \; d\Omega = \oint_{\partial\Omega_e} \phi^+ \varphi \; d\Gamma, \; \forall \phi \in \mathcal{V}_h^p. \tag{2.15}$$

Finally, the viscous part is discretized as follows. For clarity, an index notation is adopted

$$\vartheta_{ik} = \mathcal{A}_{ijkl} \partial_j \mathrm{U}_l. \tag{2.16}$$

The right-hand side of the second line of Eq. (2.10) becomes

$$\begin{aligned}\int_\Omega \partial_i \vartheta_{ik}\phi \; d\Omega &= \sum_e \left[- \int_{\Omega_e} \vartheta_{ik} \partial_i \phi \; d\Omega + \oint_{\partial\Omega_e} \phi^+ \vartheta_{ik} \widehat{n}_i \; d\Gamma \right] \\ &= \sum_e \left[- \int_{\Omega_e} (\mathcal{A}_{ijkl} \partial_j \mathrm{U}_l) \partial_i \phi \; d\Omega + \oint_{\partial\Omega_e} \phi^+ \vartheta_{ik} \widehat{n}_i \; d\Gamma \right] \\ &= \sum_e \left[\int_{\Omega_e} \partial_j (\mathcal{A}_{ijkl} \partial_i \phi) \mathrm{U}_l \; d\Omega - \oint_{\partial\Omega_e} \partial_i \phi^+ \mathcal{A}_{ijkl} \mathrm{U}_l \widehat{n}_j \; d\Gamma + \oint_{\partial\Omega_e} \phi^+ \vartheta_{ik} \widehat{n}_i \; d\Gamma \right] \\ &\simeq \sum_e \left[\int_{\Omega_e} \partial_j (\mathcal{A}_{ijkl} \partial_i \phi) \mathrm{U}_{h,l} \; d\Omega - \oint_{\partial\Omega_e} \partial_i \phi^+ \mathcal{A}^+_{ijkl} \widehat{\mathrm{U}}_l \widehat{n}_j \; d\Gamma + \oint_{\partial\Omega_e} \phi^+ \widehat{\vartheta}_{ik} \widehat{n}_i \; d\Gamma \right] \\ &= \sum_e \left[- \int_{\Omega_e} (\boldsymbol{\mathcal{A}} : \nabla_h \mathbf{U}_h) \cdot \nabla \phi \; d\Omega - \oint_{\partial\Omega_e} [\boldsymbol{\mathcal{A}}^+ : ((\widehat{\mathbf{U}} - \mathbf{U}_h^+) \otimes \widehat{\boldsymbol{n}})] \cdot \nabla \phi^+ \; d\Gamma \right. \\ &\quad \left. + \oint_{\partial\Omega_e} \phi^+ \widehat{\boldsymbol{\vartheta}} \cdot \widehat{\boldsymbol{n}} \; d\Gamma \right].\end{aligned} \tag{2.17}$$

In the last two lines, the fourth-order tensor $\boldsymbol{\mathcal{A}}$ is evaluated at the discrete solution vector. For the detailed form of $\boldsymbol{\mathcal{A}}$, the interested reader can refer to Lv (2016). The last line recovers the actual implementation in the solver, where the auxiliary variable $\boldsymbol{\vartheta}$ is not needed anymore (also referred to as the primal formulation in the literature). In the BR2 formulation, $\widehat{\mathbf{U}} = \{\mathbf{U}_h\}$ and $\widehat{\boldsymbol{\vartheta}} = \{\mathscr{P}(\boldsymbol{\mathcal{A}} : \nabla_h \mathbf{U}_h) + \eta r_e^l(\boldsymbol{\mathcal{A}} : ((\widehat{\mathbf{U}} - \mathbf{U}_h^+) \otimes \boldsymbol{n}))\}$, where $\{\cdot\}$ denotes the average across the face and r_e^l is the local lifting operator, defined on each

face, and η is a stabilization constant (equal to the number of faces). This formulation ensures the compactness of the scheme (only the information at the neighboring elements is required to advance the solution in a given element).

2.3. *Entropy-bounding stabilization method*

In a previous work (Lv *et al.* 2018), an entropy-bounded DG method was used to perform ILES of homogeneous isotropic decaying turbulence at the following conditions: $Re_\lambda = 40,\ 100$ and $Ma_t = 0.1,\ 0.6,\ 1.5$, where Re_λ is the Taylor microscale Reynolds number and Ma_t is the turbulent Mach number. The entropy-bounding stabilization method was compared to overintegration, a commonly used dealiasing method. Simulations were performed using twice as many quadrature points in each spatial direction. It was found that, in moderately to highly compressible settings ($Ma_t \geq 0.6$), overintegration was unable to stabilize the solution. This demonstrates the need for developing robust discretization and stabilization methods for highly compressible turbulent flows.

For a complete description of the entropy-bounding scheme, the reader is referred to Lv & Ihme (2015). This scheme provides mathematically provable stability for compressible inviscid flow calculations by preventing the generation of unphysical quantities. The method is based on an entropy bound that is here defined as $s_b = \ln(Cp_0/\rho_0^\gamma)$, where p_0 and ρ_0 are respectively the initial uniform pressure and density, and C is a user-input parameter. At each time step (or substage of a multistage time integration scheme), the density is limited using the procedure presented in Zhang & Shu (2011). Then, if the solution produces an entropy undershoot with respect to s_b at a quadrature point, a local (elementwise) conservative scaling operation is performed in order to correct the subcell solution in troubled elements. The element mean value is used for this operation such that ${}^{\mathcal{L}}\mathbf{U}_e = \overline{\mathbf{U}}_e + \epsilon(\mathbf{U}_e - \overline{\mathbf{U}}_e)$, where ${}^{\mathcal{L}}\mathbf{U}_e$ is the new solution in element e. ϵ is the minimum value such that the entropy of the new solution is not lower than the entropy bound at the quadrature points. The sensitivity to the user-input parameter C was also investigated. The best results were obtained for a less-restrictive bound of $C = 0.001$, even though this sensitivity was negligible for moderately compressible flows at $Ma_t = 0.6$.

2.4. *VMS SGS model*

A VMS SGS model takes advantage of the discretization to perform *a-priori* scale separation among the resolved scales. The application of this model is then restricted to the small resolved scales, using the argument of scale separation for high Reynolds number flows considering negligible interaction between the largest resolved and the unresolved scales (which are modeled in a LES). The approach of Chapelier *et al.* (2016) is followed in this work. First, the SGS model is described. Then, the multiscale framework is introduced.

Let $\mathbf{U}_h = \mathbf{U}_h^L + \mathbf{U}_h^S$, where $\mathbf{U}_h^L$ and $\mathbf{U}_h^S$ are, respectively, the large and small resolved scales. The SGS model is the classical extension of the Smagorinsky model to compressible flows

$$\begin{aligned} \boldsymbol{\tau}_{\text{SGS}} = \boldsymbol{\mathcal{T}}^D = \mu_t \left(2\boldsymbol{S} - \frac{2}{3}\text{tr}(\boldsymbol{S})\mathbf{I} \right), \\ \boldsymbol{q}_{\text{SGS}} = -C_p \frac{\mu_t}{Pr_t} \nabla \widetilde{\theta}, \end{aligned} \tag{2.18}$$

where C_p is the specific heat coefficient at constant pressure and Pr_t is a turbulent

Prandtl number. Several ways have been suggested (e.g Hughes *et al.* (2000); Farhat *et al.* (2006)) for evaluating the turbulent eddy viscosity μ_t as well as the strain-rate tensor. These include computing those quantities from the whole solution or its large or small component. The most computationally efficient way consists of using the whole solution for both quantities. This is referred to in the literature as the all-all method (Chapelier *et al.* 2016). In particular, in a DG setting, since only conservative variables are solved for, it is not straightforward to define the small part of the velocity $\boldsymbol{u}_h$, and its evaluation requires specific care, such as an additional projection to the approximation functional space. Moreover, Chapelier *et al.* (2016) compared a slightly modified version of the small-small approach to the all-all approach and found only slight differences. Therefore, we adopt this all-all approach here. With this, the eddy viscosity takes the general form

$$\mu_t = \rho(C_S\Delta)^2\sqrt{2\boldsymbol{S}:\boldsymbol{S}}, \tag{2.19}$$

where $\boldsymbol{S}$ is the symmetric part of the velocity gradient computed using the whole discrete solution available at a given time-step, meaning all the modes of the polynomial expansion are used. Here, $C_S\Delta$ is computed as $0.172\,{V_e}^{1/3}/(p+1)$, where V_e is the element volume and p is the polynomial order. The modeled term is then only applied to the small resolved scales. More precisely, if $\mathcal{V}_h^{p,L}$ and $\mathcal{V}_h^{p,S}$ denote, respectively, the large and small scales functional space, for any test function ϕ,

$$\phi = \phi^L + \phi^S,\ \phi^L \in \mathcal{V}_h^{p,L},\ \text{and}\ \phi^S \in \mathcal{V}_h^{p,S},\quad \mathcal{V}_h^{p,L} \oplus \mathcal{V}_h^{p,S} = \mathcal{V}_h^p \tag{2.20}$$

and

$$\begin{cases} \displaystyle\int_\Omega \phi^L(\partial_t\mathbf{U} + \nabla\cdot\mathbf{F} - \nabla\cdot\mathbf{Q})\ d\Omega = 0, \\ \displaystyle\int_\Omega \phi^S(\partial_t\mathbf{U} + \nabla\cdot\mathbf{F} - \nabla\cdot\mathbf{Q})\ d\Omega = \int_\Omega \phi^S\nabla\cdot\mathbf{Q}_{\text{SGS}}\ d\Omega. \end{cases} \tag{2.21}$$

Since the SGS term takes exactly the same form as the viscous term, it is discretized using the same methodology.

Finally, the spaces $\mathcal{V}_h^{p,L}$ and $\mathcal{V}_h^{p,S}$ remain to be defined. Because the test function space is generated by a tensor-product Legendre polynomial basis, the scale separation is parameterized by the partition number p_L. If ϕ_{ijk} is a basis function, it can be written $\phi_{ijk}(x,y,z) = \phi_i(x)\phi_j(y)\phi_k(z)$, where ϕ_i, ϕ_j, and ϕ_z are 1D Legendre polynomials ($i,j,k \in \{0,\dots,p\}$, where p is the maximum polynomial degree of the discretization). Therefore, we define the small scale space $\mathcal{V}_h^{p,S}$ as

$$\mathcal{V}_h^{p,S} = \{\phi_{ijk} \mid i > p_L \text{ or } j > p_L \text{ or } k > p_L\}. \tag{2.22}$$

2.5. *Some notes on post-processing of quantities involving gradients*

In the study of homogeneous isotropic turbulence, commonly used quantities to assess the solution quality are, for example, the spatial average enstrophy and the resolved dissipation as a function of time. Since the solution obtained using a DG method is discontinuous across the faces, it is relevant to discuss the method used to compute these average quantities. Specifically, for quantities that can be directly extracted from the solution vector, for instance the density or the velocity components, the most natural way is to use the same quadrature rule as the one chosen for the simulation. The quadrature rule used in this work is the Gauss-Legendre quadrature with order of accuracy $2p+7$, where p is the polynomial order of the discretization (this involves $(p+4)^3$ points, for instance, for volume integrals).

In contrast, the quantities involving gradients deserve further attention. Indeed, applying the latter method directly to the gradient of the discrete solution vector does not consider the jump of the solution across the faces. Prior comparisons for low-Mach cases with other DG solvers showed that this contribution of the discontinuities cannot be neglected, especially for quantities such as the average dilation. The BR2 formulation of Bassi *et al.* (2005), which uses the state gradient as the auxiliary vector $\boldsymbol{\vartheta}^*$, allows for a simple expression of the discrete state gradient using the lifting operator

$$\boldsymbol{\vartheta}_h^*|_{\Omega_e} = \nabla_h \mathbf{U}_h + r_e((\widehat{\mathbf{U}} - \mathbf{U}_h^+) \otimes \boldsymbol{n}), \tag{2.23}$$

using a derivation similar to the one leading to Eq. (2.14). The procedure then is to use the chain rule to express gradients as a function of state gradient components that are computed using Eq. (2.23) at the quadrature points. Integral quantities can then be evaluated using the chosen quadrature rule. Since in the present solver the auxiliary variable is the viscous flux instead, it is not completely rigorous to use the same equation. However, a comparison performed on a Taylor-Green vortex configuration with another DG solver (Renac *et al.* 2015) that used the discretization described in Bassi *et al.* (2005) showed that comparable results were obtained using Eq. (2.23). Therefore, this method will be used in this work.

3. Compressible decaying homogeneous isotropic turbulence

3.1. *Problem setup*

The configuration studied here is taken from Lee *et al.* (1991), Johnsen *et al.* (2010), and Lv *et al.* (2018). It corresponds to the decay of compressible isotropic turbulence with moderately high turbulent Mach number. This case is particularly interesting for assessing the accuracy and robustness of numerical methods because randomly distributed shocklets form during the simulation. The setup is described again here so that it can be easily reproduced with the same parameters.

The system is made dimensionless using five reference quantities: ρ_0 (initial density), $k_0 = 4\ \mathrm{m}^{-1}$ (most energetic wavenumber), u_0' (the initial root-mean-square velocity), R_g (specific gas constant), and M (molecular weight). The system is parameterized by the Taylor microscale Reynolds number $Re_\lambda = u_0'\lambda_0/\nu_0$ and the turbulence Mach number $Ma_t = \sqrt{3}u_0'/c_0$, where λ_0 is the initial Taylor microscale and c_0 is the initial speed of sound. Relevant constants are the ratio of specific heat coefficients $\gamma = 1.4$, the molecular Prandtl number $Pr = 0.7$, and the turbulent Prantdl number $Pr_t = 0.5$ for explicit SGS modeling. The eddy-turnover time is defined as $\tau_0 = \lambda_0/u_0'$. The molecular viscosity follows a power law of the form $\mu/\mu_{\mathrm{ref}} = (T/T_{\mathrm{ref}})^{0.76}$. The initial conditions are given by a divergence-free velocity field and constant thermodynamic quantities ρ_0 and p_0. The energy spectrum for the initial velocity field is prescribed as

$$E_u(k) = 16\sqrt{\frac{2}{\pi}}{u_0'}^2\frac{k^4}{{k_0}^5}\exp\left(-\frac{2k^2}{{k_0}^2}\right), \tag{3.1}$$

from which one may derive $\lambda_0 = 2/k_0 = 0.5$.

Two different Reynolds numbers are investigated, namely $Re_\lambda = 100$ and $Re_\lambda = 200$. The turbulent Mach number is fixed to $Ma_t = 0.6$. Figure 1 shows the initial and final velocity spectra as well as the LES resolution cutoffs. Increase in the Reynolds number is achieved via decreasing the molecular viscosity in the dimensionless system described previously. Therefore, two aspects make achieving DNS resolution challenging. First, the

Case	DNS	LES
$Re_\lambda = 100$	64^3 elements, $p = 3$ (256^3 DOF)	11^3 elements, $p = 5$ (66^3 DOF) 6^3 elements, $p = 5$ (36^6 DOF)
$Re_\lambda = 200$	90^3 elements, $p = 3$ (360^3 DOF)	15^3 elements, $p = 5$ (90^3 DOF) 8^3 elements, $p = 5$ (48^3 DOF)

TABLE 1. *hp*-discretization used for the DNS and LES simulations (DOF: degrees of freedom).

required number of elements increases rapidly with a decrease in maximum allowable time step size. Second, the decrease in molecular viscosity reduces the size of the shocklets, thus making it even harder to obtain complete resolution. Stabilization is required even if the grid is chosen so as to resolve the smallest turbulent length scale. We recognize that the Reynolds number might be too low for sufficient scale separation and, therefore, for an SGS model to be valuable. In fact, in the previous study of Lv *et al.* (2018), ILES approaches were adopted, and the inherent numerical dissipation of the DG scheme was sufficient to avoid any unphysical pile-up of energy. Nevertheless, this well-documented test case was chosen here in order to assess the Smagorinsky model combined with the VMS approach, both as an SGS model and as a stabilization method in a compressible setting. The authors expect that an SGS model might be required for higher Reynolds number.

A reference DNS is obtained using the DG solver. The quality of this DNS was examined and confirmed in Lv *et al.* (2018) and was conducted using 64^3 elements and a polynomial degree of $p = 3$ for $Re_\lambda = 100$. Further refinement was performed for $Re_\lambda = 200$. Entropy stabilization was found to be necessary even at this resolution for the case with high Reynolds number. The LES simulations were conducted with a polynomial degree of $p = 5$. Two reasons motivate this choice. A higher polynomial degree gives more flexibility for the VMS SGS model in the choice of the partition number. Moreover, studies by Lv *et al.* (2018) showed improvements in the solution quality when using higher polynomial order. The different *hp*-discretizations are summarized in Table 1. The ILES approach with no SGS model and entropy-bounding stabilization is compared with the VMS SGS approach at the LES resolutions. Finally, dealiasing using overintegration was necessary to achieve accuracy, especially for the ILES simulations. Therefore, a quadrature rule that is adequate to integrate polynomials of order up to $2p + 7 = 17$ was used.

3.2. *Reference data for LES*

For a fair assessment of the quality of the LES, reference data were generated from the DNS result. Two aspects must be taken into account: the lower resolution and the specifics of the DG discretization. Therefore, following the approach described in Naddei *et al.* (2018), the DNS is first filtered using a spectral cutoff filter with cutoff wavenumber equal to half the number of degrees of freedom. Then, the filtered field is projected onto a given *hp*-discretization. Finally, the reference data are generated from

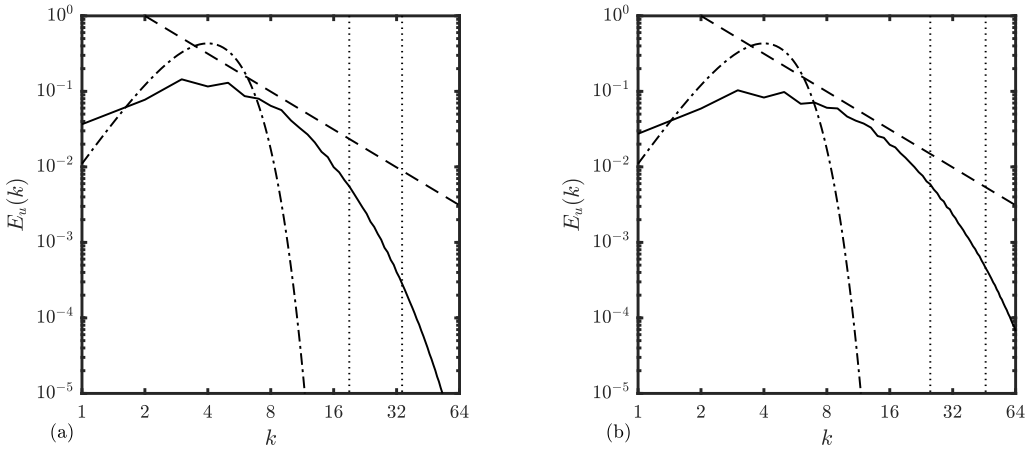

FIGURE 1. Velocity spectrum after four eddy turnover times with the LES resolution cutoff for (a) $Re_\lambda = 100$ and (b) $Re_\lambda = 200$. Solid line: velocity spectrum; dashed line: $-5/3$ slope; dotted lines: LES cutoffs; dash-dotted line: initial spectrum.

this filtered and projected DNS, referred to as FPDNS. The filtering step is important to reduce aliasing errors, especially for highly under-resolved simulations. Figure 2 shows the comparison between the DNS and FPDNS for domain averaged quantities for $Re_\lambda = 100$. Effects of filtering and projecting are rather small for the turbulent kinetic energy as well as for the density fluctuations. However, the effect on enstrophy is much more pronounced as the resolution of the LES is decreased. Therefore, it will be the primary quantity of interest for assessing the LES results.

3.3. *Statistics*

First, domain-averaged quantities are considered to assess the simulation results. Figure 3 shows the comparison between LES (with implicit and explicit SGS model) and FPDNS for $Re_\lambda = 100$ at a resolution of 11^3 elements. A standard Smagorinsky model is too dissipative, and even the kinetic energy is largely underpredicted. During the first half of the simulation, the amount of dissipation introduced by this model leads to a large overprediction of the decay rate. In fact, at this resolution, the ILES approach with entropy-bounding stabilization is a suitable approach with very little discrepancy only on the enstrophy. Similar results were obtained using a partition number of $p_L = 4$, which was sufficient to stabilize the solution. For this partition number, the SGS model is applied only to the highest modes of the DG discretization. Thus, at this resolution, the ILES approach is likely the better approach once a suitable stabilization method is incorporated into the scheme.

The results for turbulent kinetic energy and density fluctuations are quite similar for the coarser mesh with 6^3 elements (not shown here). However, as seen in Figure 4, the evolution of enstrophy is much more sensitive. In fact, the ILES approach starts to become inappropriate at this resolution, leading to overprediction of the enstrophy level. This shows that the ILES approach is likely not suited for a broad range of resolutions and is mostly effective for slightly under-resolved simulations. The best result was obtained for a VMS model at $p_L = 4$. However, at this resolution, entropy bounding was necessary to stabilize the VMS solution. This is not surprising because the SGS model does not incorporate any mechanism to detect and stabilize strong gradients. The differ-

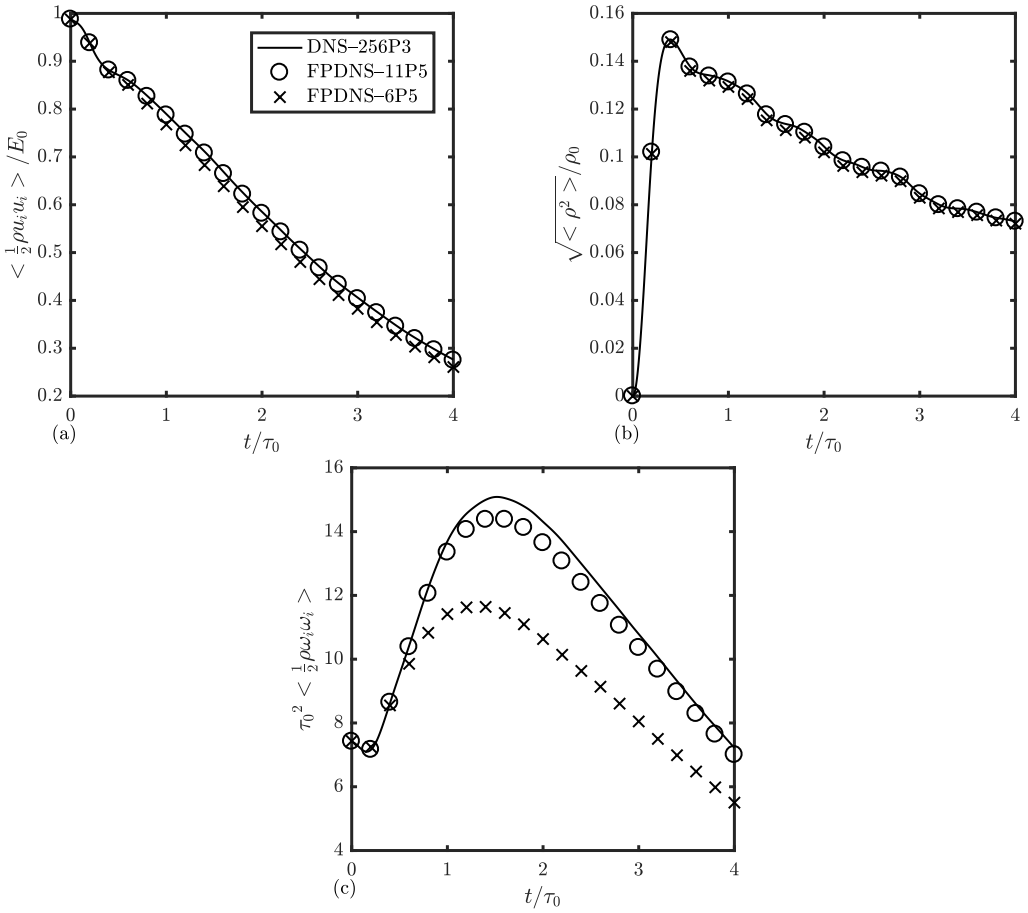

FIGURE 2. Comparison of DNS and FPDNS at $Re_\lambda = 100$: (a) turbulent kinetic energy, (b) density fluctuations, and (c) enstrophy.

ence between $p_L = 3$ and $p_L = 4$ is also evident from Figure 4, which shows excessive dissipation when $p_L = 3$. This suggests that improved results may come from a dynamic approach in which the partition number is locally and dynamically selected depending on the local resolution.

The conclusions for the higher Reynolds number $Re_\lambda = 200$ case are similar. With 15^3 elements, ILES provided satisfactory agreement (not shown here). The enstrophy level for the coarser resolution at 8^3 elements is shown in Figure 4. The VMS SGS model with $p_L = 4$ also provides the best result compared to the reference LES.

3.4. *Spectral analysis of the energy transfer*

Previous *a-priori* studies by Hughes *et al.* (2001) for incompressible turbulence showed the advantages of the VMS model compared to, for instance, the standard dynamic Smagorinsky model. They used the concept of spectral eddy viscosity to study the energy transfer from wavenumbers up to $\overline{k}$ to wavenumbers between $\overline{k}$ and k', where $\overline{k}$ is an internal cutoff and k' is the cutoff corresponding to the LES resolution, the ratio $k'/\overline{k}$ being held constant. They observed a cusp-like behavior at moderate resolution where the

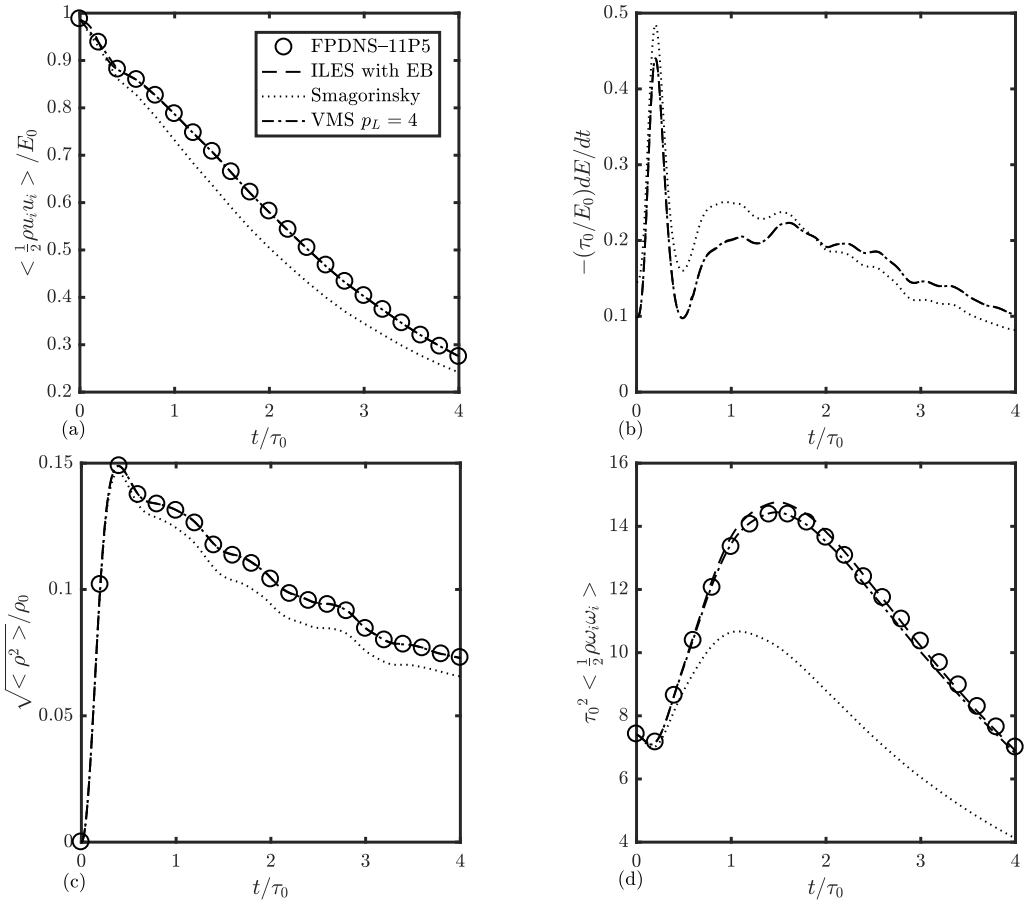

FIGURE 3. Comparison of LES (ILES and VMS including the standard Smagorinsky model) and FPDNS (reference LES) for 11^3 elements at $Re_\lambda = 100$: (a) turbulent kinetic energy, (b) decay rate, (c) density fluctuations, and (d) enstrophy.

transfer occurs only for wavenumbers close to $\overline{k}$, the large scales being almost unaffected by the unresolved scales. The VMS SGS model, which only applies SGS dissipation to a selected range of small resolved scales, was able to reproduce the correct level of energy transfer, whereas the dynamic Smagorinsky model acted on all the resolved scales, introducing too much dissipation at the largest scales. Therefore, it is of interest to know whether this behavior still remains *a-posteriori* for compressible turbulence simulations.

The energy transfer to the unresolved scales due to the model is obtained as follows. First, the discrete residual is separated into the resolved part and the SGS part

$$\frac{d\mathbf{U}_h}{dt} = \mathbf{R}_h + \mathbf{R}_h^{\text{SGS}}, \tag{3.2}$$

where $\mathbf{R}_h^{\text{SGS}}$ contains only the contribution of the model term. From the modal coefficients, the contribution of the SGS residual to the momentum equation is reconstructed and interpolated onto a structured grid. Then, using the discrete Fourier transform denoted

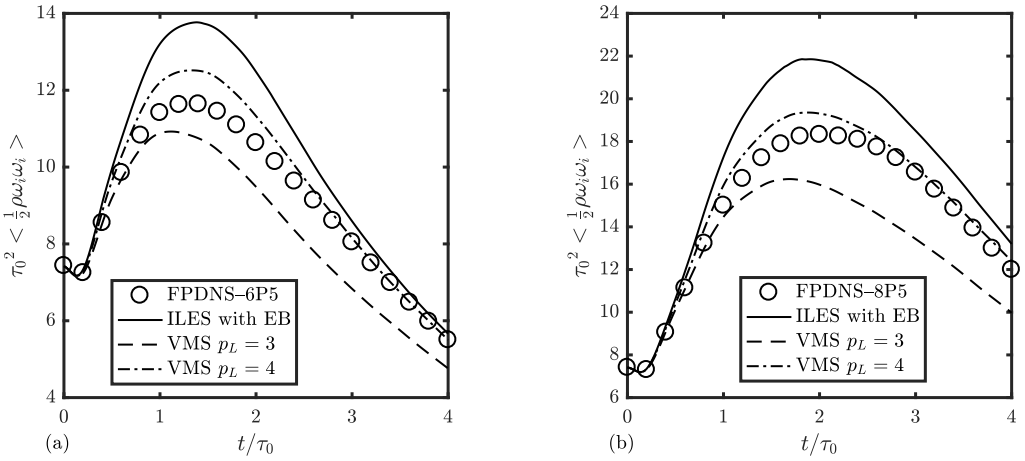

FIGURE 4. Comparison of enstrophy for LES and FPDNS: (a) $Re_\lambda = 100$ with 6^3 elements and (b) $Re_\lambda = 200$ with 8^3 elements.

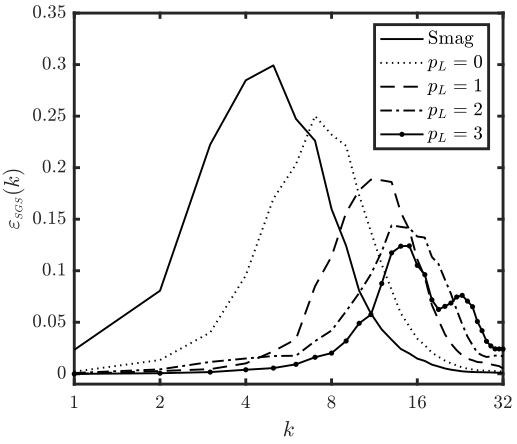

FIGURE 5. SGS dissipation spectrum at $t/\tau = 1.6$ for 11^3 elements at $Re_\lambda = 100$.

by $\widehat{\cdot}$, one obtains

$$\varepsilon_{\mathrm{SGS}}(k) = 2\Re\left[\widehat{u}_i^* \ \widehat{\frac{1}{\rho}R^{\mathrm{SGS}}_{h,u_i}}\right], \tag{3.3}$$

which corresponds to the SGS contribution to the rate of change of $\widehat{u}_i\widehat{u}_i^*/2$. Since SGS models were developed without taking into consideration the numerical dissipation inherent to the scheme, one may wonder if it affects the behavior of the model. Therefore, simulations with lower numerical dissipation were run (the upwinding in the inviscid flux as well as the penalty term in the BR2 scheme were decreased to half of their original value). The sensitivity of the model was small, suggesting that the SGS dissipation has a predominant role in the configurations considered. The convergence for the results in terms of sampling of the DG solution was verified for all the results presented in Figure 5.

Figure 5 illustrates that a VMS SGS model can restrict the range of application of the SGS dissipation to a given range of high wavenumbers. In contrast, the classical

Smagorinsky model acts mostly on low wavenumbers, which results in excessive dissipation. Such models do not take advantage of any form of inherent scale separation in the discretization *a-priori* to reduce the effect of the unresolved scales on the largest resolved scales. Increasing the partition number has two effects. First, it reduces the maximum peak of the dissipation, as the Smagorinsky coefficient is kept constant. Second, and maybe most important, the increase of the partition number leads to a shift toward the grid cutoff of the range of wavenumbers that the model acts upon.

4. Conclusions

A VMS SGS model was investigated in the context of a modal DG discretization in a compressible homogeneous isotropic turbulence setting. The ability of the SGS model to stabilize the solution and to produce accurate results was assessed in comparison with the ILES approach. For slightly under-resolved simulations, both approaches performed equally well. However, on coarser grids, the ILES approach starts to deviate from the reference LES, and the VMS SGS model produces improved results when the right partition number is chosen. These results highlight the potential for future improvement in a dynamic setting where the scale separation is chosen depending on the local resolution. For higher Reynolds numbers, the advantages of the VMS SGS approach may become even greater for flows characterized by larger scale separation. Finally, the spectral properties of the VMS model were assessed *a-posteriori*. The increase in partition number resulted in a shift of the SGS dissipation to higher wavenumbers, in agreement with previous *a-priori* studies for incompressible turbulence.

REFERENCES

Bassi, F. & Rebay, S. 2000 GMRES discontinuous Galerkin solution of the compressible Navier-Stokes equations. In Cockburn B., Karniadakis G.E. & Shu C.W. (Eds.) *Discontinuous Galerkin Methods. Lecture Notes in Computational Science and Engineering*, Vol 11. Springer, pp. 197–208.

Bassi, F., Crivellini, A., Rebay, S. & Savini, M. 2005 Discontinuous Galerkin solution of the Reynolds-averaged Navier-Stokes and k-ω turbulence model equations. *Comput. & Fluids* **34**, 507–540.

Bassi, F., Botti, L., Colombo, A., Crivellini, A., Ghidoni, A. & Massa, F. 2016 On the development of an implicit high-order discontinuous Galerkin method for DNS and implicit LES of turbulent flows. *Eur. J. Mech. B-Fluid* **55**, 367–379.

Carton de Wiart, C., Hilewaert, K., Bricteux, L. & Winckelmans, G. 2015 Implicit LES of free and wall-bounded turbulent flows based on the discontinuous Galerkin/symmertric interior penalty method. *Int. J. Numer. Methods Fluids* **78**, 335–354.

Chapelier, J.-B., de la Llave Plata & M., Lamballais, E. 2016 Development of a multiscale LES model in the context of a modal discontinuous Galerkin method. *Comput. Method. Appl. Mech. Engrg.* **307**, 275–299.

Chen, T. & Shu, C.-W. 2017 Entropy stable high order discontinuous Galerkin methods with suitable quadrature rules for hyperbolic conservation laws. *J. Comput. Phys.* **345**, 427–461.

Farhat, C., Rajasekharan, A. & Koobus, B. 2006 A dynamic variational multiscale

method for large eddy simulations on unstructured meshes. *Comput. Method. Appl. Mech. Engrg.* **195**, 1667–1691.

Fernandez, P., Nguyen, N. C. & Peraire, J. 2017 The hybridized discontinuous Galerkin method for implicit large-eddy simulation of transitional turbulent flows. *J. Comput. Phys.* **336**, 308–329.

Gassner, G. J. & Beck, A. D. 2013 On the accuracy of high-order discretizations for underresolved turbulence simulations. *Theor. Comp. Fluid. Dyn.* **27**, 221–237.

Hiltebrand, A. & Mishra, S. 2014 Entropy stable shock capturing space-time discontinuous Galerkin schemes for systems of conservation laws. *Numer. Math.* **126**, 103–151.

Hughes, T. J. R., Mazzei, L. & Jansen, K. 2000 Large eddy simulation and the variational multiscale method. *Comput. Visual. Sci.* **3**, 47–59.

Hughes, T. J. R., Mazzei, L., Overai, A. A. & Wray, A. A. 2001 The multiscale formulation of large eddy simulation: Decay of homogeneous isotropic turbulence. *Phys. Fluids* **13**, 505–512.

Johnsen, E., Larsson, J., Bhagatwala, A. V., Cabot, W. H., Moin, P., Olson, B. J., Rawat, P.S., Shankar, S. K., Sjögreenm B., Yee, H. C., Zhong, X. & Lele, S. K. 2009 Assessment of high-resolution methods for numerical simulations of compressible turbulence with shock waves. *J. Comput. Phys.* **229**, 1213–1237.

Lee, S., Lele, S. K. & Moin, P. 1991 Eddy shocklets in decaying compressible turbulence. *Phys. Fluids* **3**, 657–664.

Lesieur, M. & Compte, P. 2001 Favre filtering and macro-temperature in large-eddy simulations of compressible turbulence. *C. R. Acad. Sci. Paris II* **329**, 363–368.

Lv, Y. & Ihme, M. 2015 Entropy-bounded discontinuous Galerkin scheme for Euler equations. *J. Comput. Phys.* **295**, 715–739.

Lv, Y. 2016 *Embedded entropy concept for fluid dynamic simulations with discontinuous Galerkin scheme.* Ph.D. Thesis, Stanford University.

Lv, Y., Ma, P. C, & Ihme, M. 2018 On underresolved simulations of compressible turbulence using an entropy-bounded DG method: Solution stabilization, scheme optimization, and benchmark against a finite-volume solver. *Comput. & Fluids* **161**, 89–106.

Naddei, F., de la Llave Plata, M., Lamballais, E., Couaillier, V., Massot, M. & Ihme, M. 2018 Large-scale space definition for the DG-VMS method based on energy transfer analyses. *Proceedings of the Summer Program*, Center for Turbulence Research, Stanford University.

Renac F., de la Llave Plata M., Martin E., Chapelier J.-B. & Couaillier V. 2015 Aghora: A high-order DG Solver for turbulent flow simulations. In Kroll N., Hirsch C., Bassi F., Johnston C. & Hillewaert K. (Eds.) *IDIHOM: Industrialization of High-Order Methods – A Top-Down Approach*, Vol. 128. Springer, pp. 315–335.

Zhang, X. & Shu, C.-W. 2011 Positivity-preserving high order discontinuous Galerkin schemes for compressible Euler equations with source terms. *J. Comput. Phys.* **230**, 1238–1248.